 doi:10.20944/preprints202206.0419.v1

Article

Local Heat Transfer Dynamics in the In-Line Tube Bundle under Asymmetrical Pulsating Flow

Aigul Haibullina [1,*], Aidar Khairullin [1,*], Denis Balzamov [1], Vladimir Ilyin [1], Veronika Bronskaya [2,3], Liliya Khairullina [3]

[1] Kazan State Power Engineering University, 51 Krasnoselskaya Str., 420066 Kazan, Russia; dbalzmov@mail.ru (D.B.); ilyinvk@mail.ru (V.I.)
[2] Kazan National Research Technological University, 68, Karl Marx Street, Kazan, 420015, Russian; VVBronskaya@kpfu.ru (V.B.)
[3] Kazan Federal University, 18, Kremlyovskaya str, Kazan, 420008 Kazan, Russia; Liliya.Hajrullina@kpfu.ru (L.K.)
* Correspondence: haybullina.87@mail.ru (A.H.); kharullin@yandex.ru (A.K.)

Abstract: The pulsating flow is one of the techniques which can enhance heat transfer, therefore leading to energy saving in tubular heat exchangers. This paper investigates the heat transfer and flow characteristics in a two-dimensional in-line tube bundle with the pulsating flow by a numerical method using the Ansys Fluent. Numerical simulation is performed for Reynolds number Re = 500 with different frequencies and amplitude of pulsation. Heat transfer enhancement was estimated from the central tube of the tube bundle. Pulsation velocity had an asymmetrical character with a reciprocating flow. The technique developed by the authors to obtain asymmetric pulsations was used. This technique allows simulating an asymmetric flow in heat exchangers equipped with a pulsation generation system. Increase in both the amplitude and the frequency of the pulsations has a significant effect on heat transfer enhancement. Heat transfer enhancement is mainly observed in the front and back of the cylinder. At a steady flow in these areas, heat transfer is minimal due to the weak circulation of the flow. The increase in heat transfer in the front and back of the cylinder is associated with increased velocity and additional flow mixing in these areas.

Keywords: asymmetric pulsating flow; in-line tube bundle; CFD; enhancement of heat transfer

1. Introduction

Cross-flow tube bundles are widely used in various heat exchange equipment. Shell and tube heat exchangers are commonly used in the power, food, chemical, and petrochemical industries. Therefore, improving the efficiency of such equipment can lead to significant energy savings. Improving the efficiency of shell-and-tube heat exchangers is closely related to heat transfer enhancement techniques. The use of various techniques for heat exchange augmentation can lead to a decrease in the metal consumption of heat exchange equipment, a reduction in the capacities required for pumping, and a decrease in the consumption of heat carriers. The accumulated literature in this area includes thousands of references and continues to grow [1-5].

Both passive and active techniques are used to heat transfer enhancement. Passive methods include twisted tube bundles [6], tubes with spiral grooves [7], tubes with spiral finning [8], tube bundles with different diameters [9], etc. The active method includes the application of an electromagnetic field [10], vibration [11], or rotation [12] of the heat exchange surface, etc.

Artificially created pulsation of the fluid flow is one of the active heat transfer enhancement techniques. Many authors [13-16] studied pulsating flows to enhance heat transfer. Kikuchi et al. [17] studied the heat transfer of a single cylinder in a pulsating flow numerically and experimentally. The work [17] showed that increasing the frequency and amplitude of pulsations leads to heat transfer enhancement. The increase in

 doi:10.20944/preprints202206.0419.v1

heat transfer occurs at the front and back of the cylinder. The maximum values of the instantaneous Nusselt number are observed at pulsation phases corresponding to the maximum flow velocity. Fu et al. and Zheng et al. [18,19] investigated the heat transfer of a single cylinder in a pulsating flow numerically. Authors [18] conclude that heat transfer increases when the forced pulsation frequencies are synchronized with the natural frequencies of vortex oscillations (the phenomenon of vortex resonance) [20]. Heat transfer enhancement is mainly observed in the back of the cylinder, in work [19] in the front of the cylinder. Heat transfer increases with an increase in the pulsating frequency. When the forced pulsation frequencies are two times higher than the natural frequencies of vortex oscillations, the enhancement of heat transfer has a maximum value. A further increase in the pulsation frequency leads to a decrease in heat transfer intensification. The authors [17-19] noted that the maximum instantaneous values of the Nusselt number are observed at pulsation phases corresponding to the maximum flow velocities. The heat transfer of a single square cylinder in a pulsating flow was experimentally investigated by Ji et al. [20]. The maximum enhancement of heat transfer is observed when the pulsation frequencies are twice as high as the natural frequencies of the vortex oscillations. In the article [21], the effect of an oscillating cylinder on heat transfer was investigated numerically. It is shown that heat transfer increase with increasing amplitude and frequency of pulsations. The field synergy principle was applied to study heat transfer enhancement mechanisms. It was found that streamlines become disordered behind the cylinder with increasing amplitude. With increasing frequency, the intensity of the vortices behind the cylinder increases. The authors [22,23] analyzed the formation of vortex structures in the wake of a single cylinder in a pulsating airflow. A relationship between vortex structures with heat exchange was established. It is shown that the maximum heat transfer augmentation is observed in the cylinder back, which corresponds to the flow regime with the formation of two symmetric vortices in the cylinder wake. The authors associate the increase in heat transfer with the disturbing flow structure in the back of the cylinder. The authors are determined [24,25] the flow and heat transfer characteristics of in-line and staggered tube bundles at symmetric air pulsations. Flow pulsations lead to an increase in heat transfer due to the disturbing vortex flow structures in the annular space of the tube bundles. For the in-line tube bundle, the maximum increase in heat transfer was 42% for the staggered tube bundle, 16%. Liang et al. [26] studied pulsating sinusoidal flows in an in-line tube bundle numerically using the large eddy simulation (LES) technique. Increase in heat transfer from the cylinder of the first and second rows is obtained, which is associated with the phenomenon of vortex resonance. Wu et al. [27] experimentally investigated the external heat exchange of a staggered tube bundle immersed in water. In this study, the situation of a heat exchanger immersed in seawater was simulated. It was found that increase in the amplitude is practically proportional to increase in the heat transfer of the tube bundle. A change in the wave frequency has almost no effect on the heat transfer augmentation. Authors [28] numerically investigated heat transfer at symmetric pulsations in a staggered tube bundle. It is shown that heat transfer augmentation changed with the pulsations regime and the row of the tube bundle. Mulcahey et al. [29] investigated the heat transfer of a ten-row tandem of square tubes with symmetric flow pulsations. Results are presented for different tube spacing. It is shown that the heat transfer depends on the geometry and flow regimes.

Hydrodynamics and heat transfer in a transverse flow around tube bundles in a steady flow has been well studied [30-33]. However, there are very few similar studies with pulsating flows. Most of the work is devoted to a single cylinder. In the case of pulsating flows, at least two more are added to the similarity criteria used in a steady flow: the Strouhal number and the amplitude of the pulsations, which complicates the study even for a single cylinder. The problem is more complicated for bundles of tubes by the sheer number of configurations encountered in practice. In the works related to the research topic, the pulsations are symmetrical. Mechanisms of heat transfer augmentation have not been fully revealed [34]. Many researchers conclude that the intensi-

Preprints (www.preprints.org) | NOT PEER-REVIEWED | Posted: 30 June 2022 doi:10.20944/preprints202206.0419.v1

fication of heat transfer in pulsating flows is associated with the phenomenon of vortex resonance [20,35-37]. Also, authors [17,19,22,24,38,39] mentioned the restructuring of the flow structure, a decrease in the boundary layer, mixing of large-scale vortex structures, and additional turbulization of the flow.

This work investigates the mechanisms leading to heat transfer enhancement in the in-line tube bundle with asymmetric flow pulsations. Numerical simulations are presented for the Strouhal number Sh 0.038, 0.057, 0.114, amplitude A/D 1.25, 3, 4.5, and Reynolds number Re 500.

2. Mathematical model

2.1. Computational domain and boundary conditions

The computational domain of the model is a bundle of tubes (figure 1), which is bounded on all sides by halves of tubes. The diameter of the tubes is D= 0.01 m. The relative transverse and longitudinal pitch are $s_{1,2}/D$ = 1.3. The 2D in-line tube bundle was employed to simplify the mathematical model. Satisfactory agreement with experimental data with 2D formulation was obtained in [28,40,41] for systems similar to the flow field studied in this work. A constant temperature t_w = 42 °C and a no slip condition (U_x = 0, U_y = 0) were set on all walls of the tubes. A constant flow temperature t_f = 27 °C was set to the computational domain at the inlet. Symmetry condition ($\partial U_x/\partial n$ = 0, $\partial U_y/\partial n$ = 0, $\partial p/\partial n$ = 0) on top and bottom of domain. At the outlet, constant pressure P = 101325 Pa. Water was chosen as the working fluid. The thermophysical properties of water were calculated depending on the flow temperature.

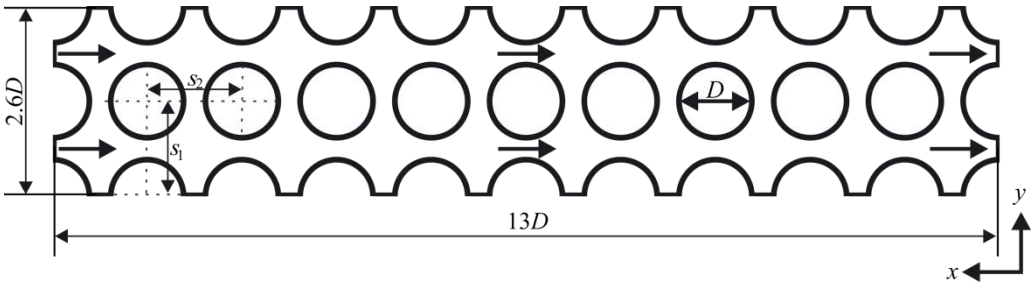

Figure 1. The computational domain.

For a steady flow at the inlet to the computational domain, a constant flow velocity u was set corresponding to the Reynolds numbers Re = 500. The Reynolds numbers were calculated as follows:

$$Re = Du/\eta,$$

where η is the kinematic viscosity of water. The pulsating asymmetric flow at the inlet of the computational domain was set according to figure 2. The asymmetric flow corresponded to the required frequency f and the dimensionless relative amplitude A/D of pulsations, where A is dimensional amplitude was found by the equation:

$$A = \langle u_p \rangle \tau \text{ m},$$

where $\langle u_p \rangle$ is pulsation flow velocity averaged overtime τ for the corresponding negative values of instantaneous pulsation velocity u_p:

$$\langle u_p \rangle = \frac{\int_{\tau_1}^{\tau_2} u_p d\tau}{\tau_2 - \tau_1}.$$

Preprints (www.preprints.org) | NOT PEER-REVIEWED | Posted: 30 June 2022 doi:10.20944/preprints202206.0419.v1

The pulsating frequency was found by the equation:

$$f = 1/T \text{ Hz},$$

where T is the pulsation period consisting of two half periods:

$$T = T_1 + T_2 \text{ s},$$

where T_1 is the first pulsation half-period, T_2 is second half-period. The steady flow velocity u_{st} was equal to the pulsation flow velocity $\langle u_p \rangle$ averaged over the pulsation period:

$$u_{st} = \langle u_p \rangle = \frac{\int_0^T u_p d\tau}{T}.$$

The Strouhal number defined as:

$$Sh = fD/u.$$

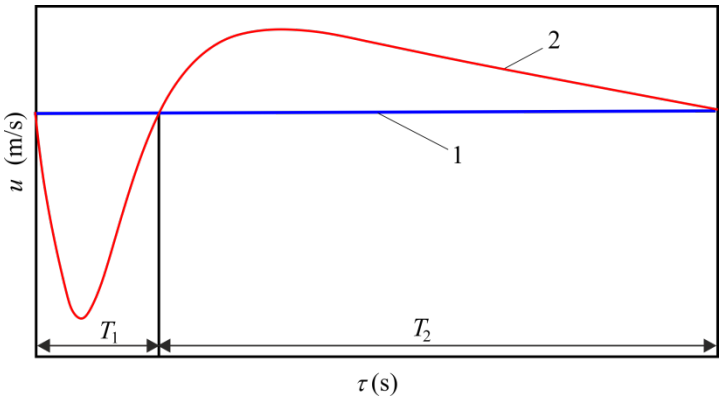

Figure 2. Pulsating asymmetric flow: 1 – steady flow; 2 – pulsating velocity.

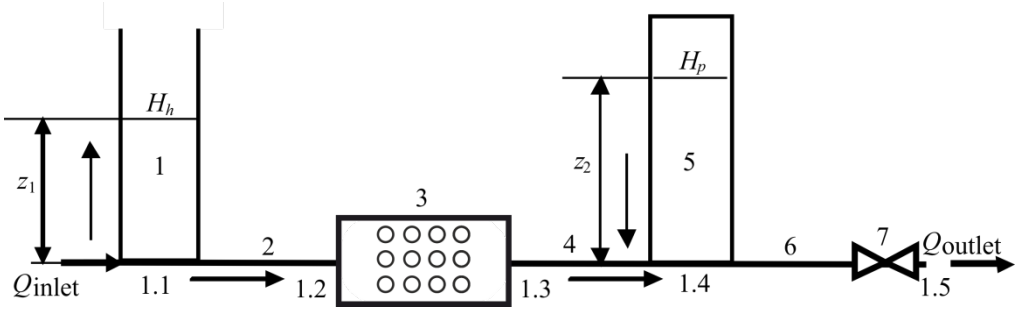

Figure 3. Scheme of hydraulic model for generating a pulsating flow: 1 - hydraulic accumulator, 2,4,6 - pipes, 3 - tube bundle, 5 - pulsation chamber, 7 -valve.

Pulsation velocity had an asymmetrical character with a reciprocating flow. The technique developed by the authors to obtain asymmetric pulsations was used. This technique simulates an asymmetric flow in heat exchangers equipped with a pulsation generation system [42]. Figure 3 shows a scheme of hydraulic model for generating a pulsating flow with a reciprocating flow in a tube bundle. The geometric parameters of the system elements for generating pulsations flow in the tube bundle corresponded to the experimental setup parameters [42].

To find the change in flow rates and pressure over time, a system of differential-algebraic equations (1-8) was solved. The flow rate at nodes 1.1-1.5 is defined by equations:

 doi:10.20944/preprints202206.0419.v1

$$Q_{\text{inlet}} - Q_1 - Q_2 = 0, \tag{1}$$

$$Q_4 - Q_5 - Q_6 = 0, \tag{2}$$

where Q is the volumetric flow rate of hydraulic model elements. The flow rate in the hydraulic accumulator 1 is defined by relation:

$$\frac{dQ_1}{d\tau} = gS_1 \frac{H_1 - (H_h + z_1)}{z_1} - \left[\frac{k_1}{2D_{j1}S_1} + \left(\frac{S_1}{S_{h0}} \right)^2 \right] Q_1 |Q_1|, \tag{3}$$

$$\frac{dz_1}{d\tau} = \frac{Q_1}{S_1}, \tag{4}$$

where H_1 and H_h are pressure in node 1.1 and on the surface of the liquid in the hydraulic accumulator 1. S_{h0} is connecting hole area with node 1.1 at the bottom of the hydraulic accumulator. D_j, k and S are the diameter, area and hydraulic resistance coefficient of hydraulic model elements respectively. g = 9,8 is gravity acceleration. z_1 is the liquid level in the hydraulic accumulator.

The flow rate in pipes 2,4 and tube bundle 3 is defined by the relation:

$$\left(\frac{l_2}{S_2} + \frac{l_3}{S_3} + \frac{l_4}{S_4} \right) \frac{dQ_2}{d\tau} = gS_2(H_1 - H_4) - Q_2|Q_2| \left(\frac{k_2 l_2}{2D_{j2}S_2} + \frac{k_3 l_3}{2D_{j3}S_3} + \frac{k_4 l_4}{2D_{j4}S_4} \right), \tag{5}$$

where l is length of hydraulic model elements.

The flow rate in the pulsation chamber 5 was carried out by following relations:

$$\frac{dQ_5}{d\tau} = gS_5 \frac{H_4 - z_2 - H_p}{z_2} - \left[\frac{k_5}{2D_{j5}S_5} + \left(\frac{S_5}{S_{p0}} \right)^2 \right] Q_5 |Q_5|, \tag{6}$$

$$\frac{dz_2}{d\tau} = \frac{Q_5}{S_5}, \tag{7}$$

where S_{p0} is connecting hole area with node 1.5 at the bottom of the pulsation chamber. H_4 and H_p are pressure in node 1.4 and on the surface of the liquid in the pulsation chamber 5. z_2 is the liquid level in the pulsation chamber.

The flow rate in the in the pipes 6 is defined by relations:

$$\frac{l_6}{S_6} \frac{dQ_6}{d\tau} = g(H_4 - H_h) - Q_6|Q_6| \left(k_6 \frac{l_6}{D_{j6}S_6^2} + k_7 \frac{1}{S_7^2} \right). \tag{8}$$

The coefficient of hydraulic resistance k was found according to empirical formulas [46]. The required flow rate was set at the inlet of the hydraulic model. The pressure dependence on time $H_P(t)$ was set to generate a pulsating flow in the pulsating chamber. The shape of the $H_P(t)$ dependence was obtained on an experimental setup in [42]. The system of equations (1-8) was solved by Newton's iterative method [43].

In figure 4, the results obtained by solving equations (1–8) are compared with the experimental data [42]. The obtained results are in good agreement with the experimental data; the deviation from the calculated data was 2%.

Preprints (www.preprints.org) | NOT PEER-REVIEWED | Posted: 30 June 2022 doi:10.20944/preprints202206.0419.v1

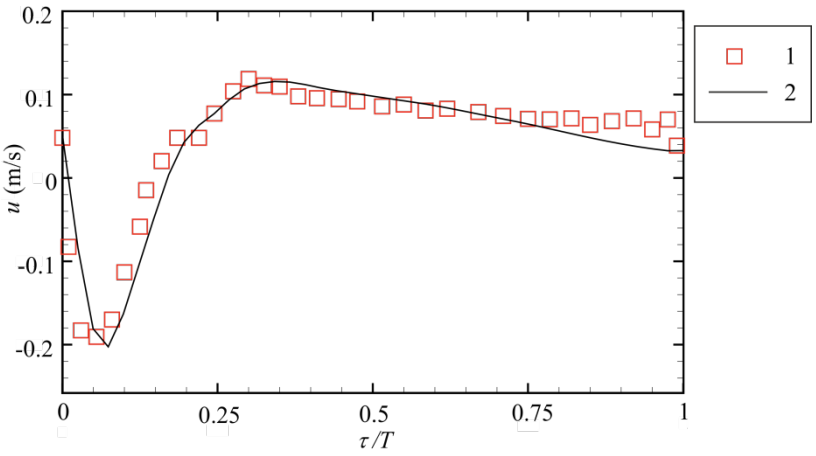

Figure 4. Pulsating velocity at f = 0.5 Hz, A/D = 3, Re = 500: 1 - experimental data [45]; 2 - numerical simulation.

2.2. Modeling Approach

The flow of an incompressible fluid was calculated by the Reynolds averaged Navier-Stokes equation. The simple one-equation model Spalart–Allmaras (SA) [44] was used as a turbulence model, which requires a lower computational cost. A comparative analysis of the SA model and the LES for a fluid flow in a tube bundle was carried out by Wang et al. [45]. As a result, it was shown that the SA model in a two-dimensional setting could predict flow characteristics. The maximum mesh size related to the tube diameter was y_{max}/D = 0.2. The minimum cell size in the near-wall region is $r_{min}/D = 3.16 \cdot 10^{-2}$. The grid size in the near-wall region expanded in the radial direction with a factor of 1.2. The number of layers in the near-wall region was 10. The convergence of a grid solver with similar systems to this work was carried out by Kim et al. and Mulcahey et al. [29,46]. In present study, the maximum mesh size was 0.2 mm. In works [29,46], a sufficient element size was 0.2 mm and higher. Mathematical modeling was carried out in Ansys Fluent, with a coupled solution algorithm based on the Pressure-Based solver. For all calculations, the SIMPLE algorithm was used. Except for the energy equation, residual was less than 10^{-4} for all governing equations. A convergence criterion of 10^{-6} was used for the energy equation for residuals. Time step was 0.01 s. For time stepping the first order implicit transient formulation was used.

2.3. Methodology for evaluating results of simulation

The flow and heat transfer characteristics used in the analysis of the obtained results were calculated for the central cylinder in the fifth row of the tube bundle. The heat flux q averaged over the surface of the wall q_o was found by equation (9), over the surface, and over time $\langle q_o \rangle$ using equation (10). Local heat flux q_φ averaged depending on the azimuth angle – φ (figure. 5) by equation (11), q_φ averaged over time by equation (12).

$$q_o = \frac{\int_0^{360} q d\varphi}{\pi D}, \tag{9}$$

$$\langle q_o \rangle = \frac{\int_0^{T} q_o d\tau}{T}, \tag{10}$$

Preprints (www.preprints.org) | NOT PEER-REVIEWED | Posted: 30 June 2022 doi:10.20944/preprints202206.0419.v1

$$q_\varphi = \frac{\int_{\varphi_1}^{\varphi_2} q d\varphi}{\pi D/8}, \tag{11}$$

$$\langle q_\varphi \rangle = \frac{\int_0^T q_\varphi d\tau}{T}. \tag{12}$$

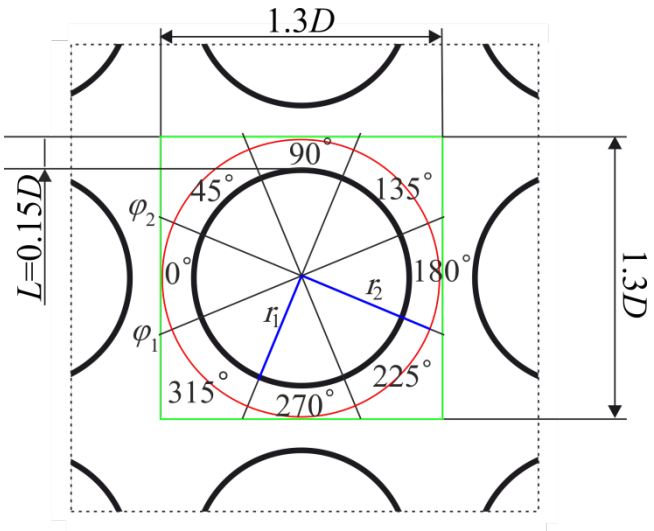

Figure 5. Location of the azimuth angle and the annular region around the cylinder of the fifth row of the tube bundle to determine the flow characteristics and heat transfer.

The temperature of water t_s was averaged over the area around the cylinder for $x = [0; 1.3D]$ $y = [0; 1.3D]$ (Figure. 5) and was found by equation (13). The temperature averaged over space and time $\langle t_s \rangle$ was found by equation (14).

$$t_s = \frac{\int_{y_1}^{y_2}\int_{x_1}^{x_2} t dx dy}{(1.3D)^2 - \pi D^2/4}, \tag{13}$$

$$\langle t_s \rangle = \frac{\int_0^T t_s d\tau}{T}. \tag{14}$$

The velocity U was found according to equation (15). The velocity U_a averaged over the sector area around the cylinder with the thickness $L = 0.15D$ (Figure 5) was found according to equation (16), over space and time $\langle U_a \rangle$, according to equation (17). The local fluid velocity U_φ is averaged depending on the azimuth angle φ according to equation (18), U_φ is time-averaged $\langle U_\varphi \rangle$ according to equation (19).

$$U = |U| = \sqrt{U_x^2 + U_y^2}, \tag{15}$$

where $U_{x,y}$, is the velocity components.

$$U_a = \frac{\int_{r_1}^{r_2}\int_0^{360} U d\varphi dr}{F(\varphi, r)}, \tag{16}$$

Preprints (www.preprints.org) | NOT PEER-REVIEWED | Posted: 30 June 2022 doi:10.20944/preprints202206.0419.v1

where $F(\varphi,r)$ is the area of the sector around the cylinder.

$$\langle U_a \rangle = \frac{\int_0^T U_a d\tau}{T}, \tag{17}$$

$$U_\varphi = \frac{\int_{r_1}^{r_2}\int_{\varphi_1}^{\varphi_2} U d\varphi dr}{F(\varphi,r)}, \tag{18}$$

$$\langle U_\varphi \rangle = \frac{\int_0^T U_\varphi d\tau}{T}. \tag{19}$$

The effective thermal conductivity λ_{eff} averaged over the annular region around the cylinder $\lambda_{eff,a}$, a was determined by equation (20), over space and time $\langle \lambda_{eff,a} \rangle$ by equation (21). Local effective thermal conductivity $\lambda_{eff,\varphi}$ and local effective thermal conductivity averaged over time $\langle \lambda_{eff,\varphi} \rangle$ according to equations (22), (23).

$$\lambda_{eff,a} = \lambda_a + \lambda_{turb,a}, \tag{20}$$

$$\langle \lambda_{eff,a} \rangle = \langle \lambda_a \rangle + \langle \lambda_{turb,a} \rangle, \tag{21}$$

$$\lambda_{eff,\varphi} = \lambda_\varphi + \lambda_{turb,\varphi}, \tag{22}$$

$$\langle \lambda_{eff,\varphi} \rangle = \langle \lambda_\varphi \rangle + \langle \lambda_{turb,\varphi} \rangle, \tag{23}$$

where λ, λ_{turb} were thermal and turbulent thermal conductivity of the water. λ, λ_{turb} in equations (20)-(23) was defined similarly to equations (16)-(19).

The temperature difference Δt was found according to equation (24), averaged over time $\langle \Delta t \rangle$ according to equation (25).

$$\Delta t = t_{wall} - t_s, \tag{24}$$

$$\langle \Delta t \rangle = t_{wall} - \langle t_s \rangle. \tag{25}$$

The Nusselt number averaged over space Nu_o was found according to equation (26), over space and time $\langle Nu_o \rangle$ according to equation (26), (27). The local Nusselt number averaged over one-eighth of the region around the cylinder Nu_φ and over time $\langle Nu_\varphi \rangle$ were determined by the equations (28), (29).

$$Nu_o = \frac{q_o D}{\Delta t \lambda_a}, \tag{26}$$

$$\langle Nu_o \rangle = \frac{\langle q_o \rangle D}{\Delta t \langle \lambda_a \rangle}, \tag{27}$$

$$Nu_\varphi = \frac{q_\varphi D}{\Delta t \lambda_\varphi}, \tag{28}$$

$$\langle Nu_\varphi \rangle = \frac{\langle q_\varphi \rangle D}{\Delta t \langle \lambda_\varphi \rangle}. \tag{29}$$

Preprints (www.preprints.org) | NOT PEER-REVIEWED | Posted: 30 June 2022 doi:10.20944/preprints202206.0419.v1

2.4. Model verification

In work [47] a comparative evaluation of the applicability of various RANS models for modeling heat transfer in an in-line tube bundle at a steady flow was carried out. SA, Shear Stress Transport (SST), and Reynolds Stress Model (RSM) were compared with empirical correlation [32]. Models showed good agreement with the empirical correlation. The difference in heat transfer at Reynolds number 500 for SA, SST, and RSM models with the empirical correlation was 12.6%, 14.6%, and 11.5%, respectively. The SA model was chosen to simulate the pulsating flow taking into account its computational cost. Figure 6 shows the results of numerical simulation and experimental data [42] for the pulsating flow at the Reynolds number of 500. According to figure 6 the numerical simulation results are in agreement with experimental data. The experimental and numerical simulation difference averaged 17%, with an experimental data error of 12%.

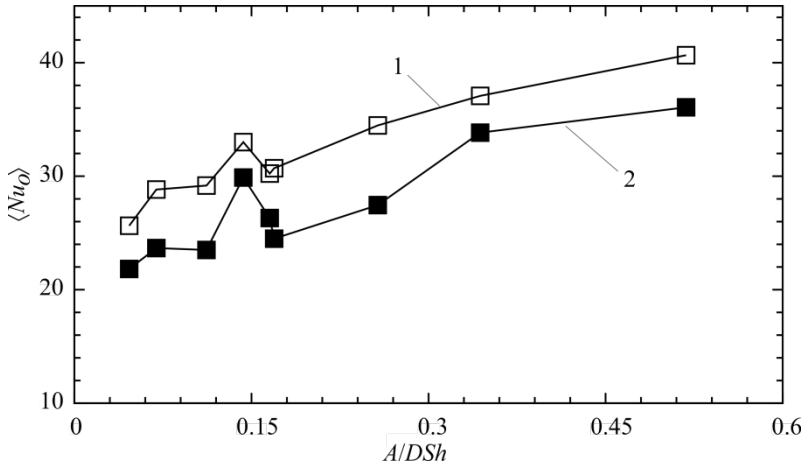

Figure 6. Variation of $\langle Nu_o \rangle$ with A/DSh: 1 – experimental data [42]; 2 - numerical simulation.

3. Results and Discussions

Simulations are performed for the amplitude of the pulsations A/D 1.25, 3, 4.5, the pulsation frequency f 0.166 Hz, 0.25 Hz, 0.5 Hz, the Strouhal number Sh 0.038, 0.057, 0.114, the Prandtl number Pr = 6.2, and the Reynolds number Re = 500.

3.1. Effect of amplitude and frequency of pulsations on flow and heat transfer characteristics

Figure 7 shows the effect of the amplitude A/D and the pulsation frequency f on the augmentation in the velocity $\langle \delta U_a \rangle = \langle U_{a,p} \rangle / U_{a,st}$, heat flux $\langle \delta q_o \rangle = \langle q_{o,p} \rangle / q_{o,st}$, Nusselt number $\langle \delta Nu_o \rangle = \langle Nu_{o,p} \rangle / Nu_{o,st}$, temperature difference $\langle \delta \Delta t \rangle = \langle \Delta t_p \rangle / \Delta t_{st}$ and effective thermal conductivity $\langle \delta \lambda_{eff,a} \rangle = \langle \lambda_{eff,a,p} \rangle / \lambda_{eff,a,st}$. The velocity, heat flux, Nusselt number, and effective thermal conductivity are higher with higher amplitude. The temperature difference is almost the same (change less than 0.2%). Augmentation of heat transfer with increase in the amplitude of pulsations correlates with increase in the flow velocity and the effective thermal conductivity. The temperature difference stays the same (change less than 0.3%), with increased pulsation frequency, while increase in heat flux and velocity is observed. The increase in the effective thermal conductivity is no more than 0.5%. The maximum increase in heat transfer was 57% at f = 0.5 Hz (Sh = 0.114), A/D = 4.5, which is consistent with the data of other authors. In paper [24], with symmetric pulsations in the in-line tube bundle, an augmentation of 42% was obtained at Sh = 0.3. In paper [27], at higher amplitudes A/D = 18.5, a heat transfer augmentation of 200% was achieved.

Preprints (www.preprints.org) | NOT PEER-REVIEWED | Posted: 30 June 2022 doi:10.20944/preprints202206.0419.v1

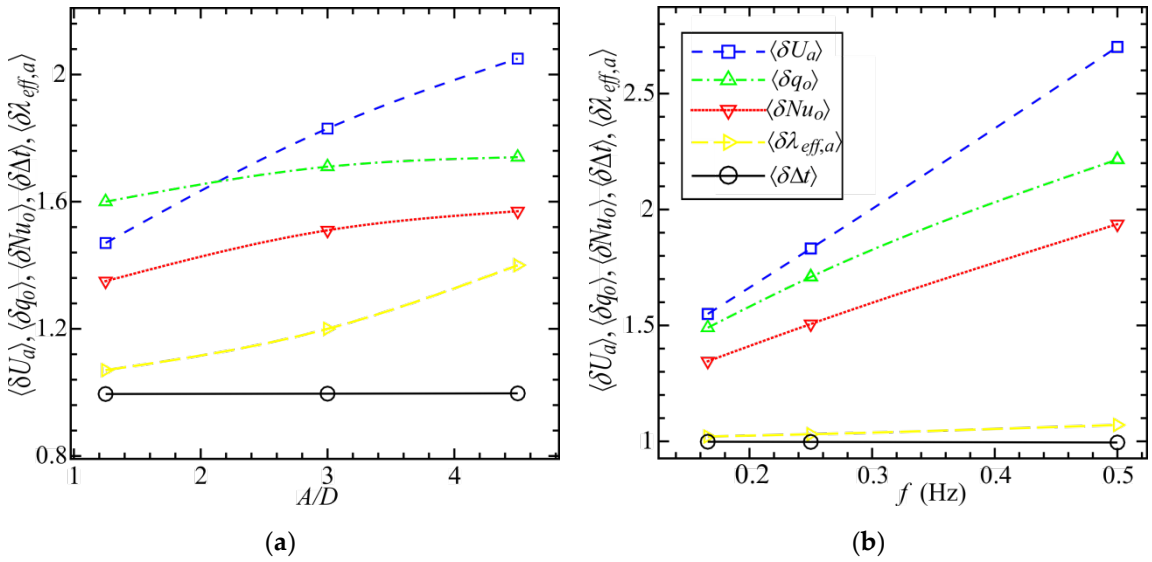

Figure 7. Effect of pulsations on flow and heat transfer characteristics: (**a**) Variation of $\langle \delta U_a \rangle$, $\langle \delta q_o \rangle$, $\langle \delta Nu_o \rangle$, $\langle \delta \Delta t \rangle$, $\langle \delta \lambda_{eff,a} \rangle$ with A/D at f = 0.25 Hz; (**b**) Variation of $\langle \delta U_a \rangle$, $\langle \delta q_o \rangle$, $\langle \delta Nu_o \rangle$, $\langle \delta \Delta t \rangle$, $\langle \delta \lambda_{eff,a} \rangle$ with f at A/D = 3.

Figure 8 shows the dynamics of δU_a, δq_o, δNu_o, $\delta \Delta t$ and $\delta \lambda_{eff,a}$ for one period of pulsations at frequency f = 0.5 Hz. When considering the dynamics of instantaneous values of increases in effective thermal conductivity and the Nusselt number over time, two peaks are observed (figure 8, (b), (e)). The first peak is observed up to τ/T = 0.25, which corresponds to the first half-period of pulsations T_1, the second peak is observed after τ/T = 0.25, which corresponds to the second half-period of pulsations T_2. The fluid flow in the tube bundle is characterized by a reciprocating flow. Therefore, the first maximum of the values δNu_o and $\delta \lambda_{eff,a}$, is associated with the acceleration of the fluid flow during its flow in the opposite direction (figure 4). The second maximum is related to the acceleration of the fluid flow during its flow in the forward direction (second half-period of pulsations T_2). For instantaneous values of heat flux and velocity (figure 8, (a), (c)) there is one significant peak during the T_1 and the second less noticeable during T_2. Both peaks are also associated with the accelerations of the fluid flow from pulsation. The more significant value of the first velocity peak (figure 8, (c)) is associated with the asymmetric nature of the flow pulsations at the inlet to the computational domain. Maximum velocity amplitude values at tube bundle inlet are higher at the first half-period of pulsation than the second half-period of pulsation. Velocity amplitude values are the difference between steady flow velocity and instantaneous pulsating velocity. Differences between velocity amplitude values are higher with higher pulsations amplitude A/D. At the minimum value of the pulsations amplitudes A/D=1.25, the velocity values of the peaks are close (figure 8, (c)). Obviously, with decreasing pulsations amplitude, the peak of the first half-period of pulsation will become smaller than the peak of the second half-period of pulsation.

A decrease in the instantaneous values of the temperature difference $\delta \Delta t$ during the first half-period of pulsations is caused by the reversal flow. The increase in heat transfer with increase in the instantaneous velocity at asymmetric pulsations correlates with the data of other authors [17-19], where the pulsations were symmetric.

Preprints (www.preprints.org) | NOT PEER-REVIEWED | Posted: 30 June 2022 doi:10.20944/preprints202206.0419.v1

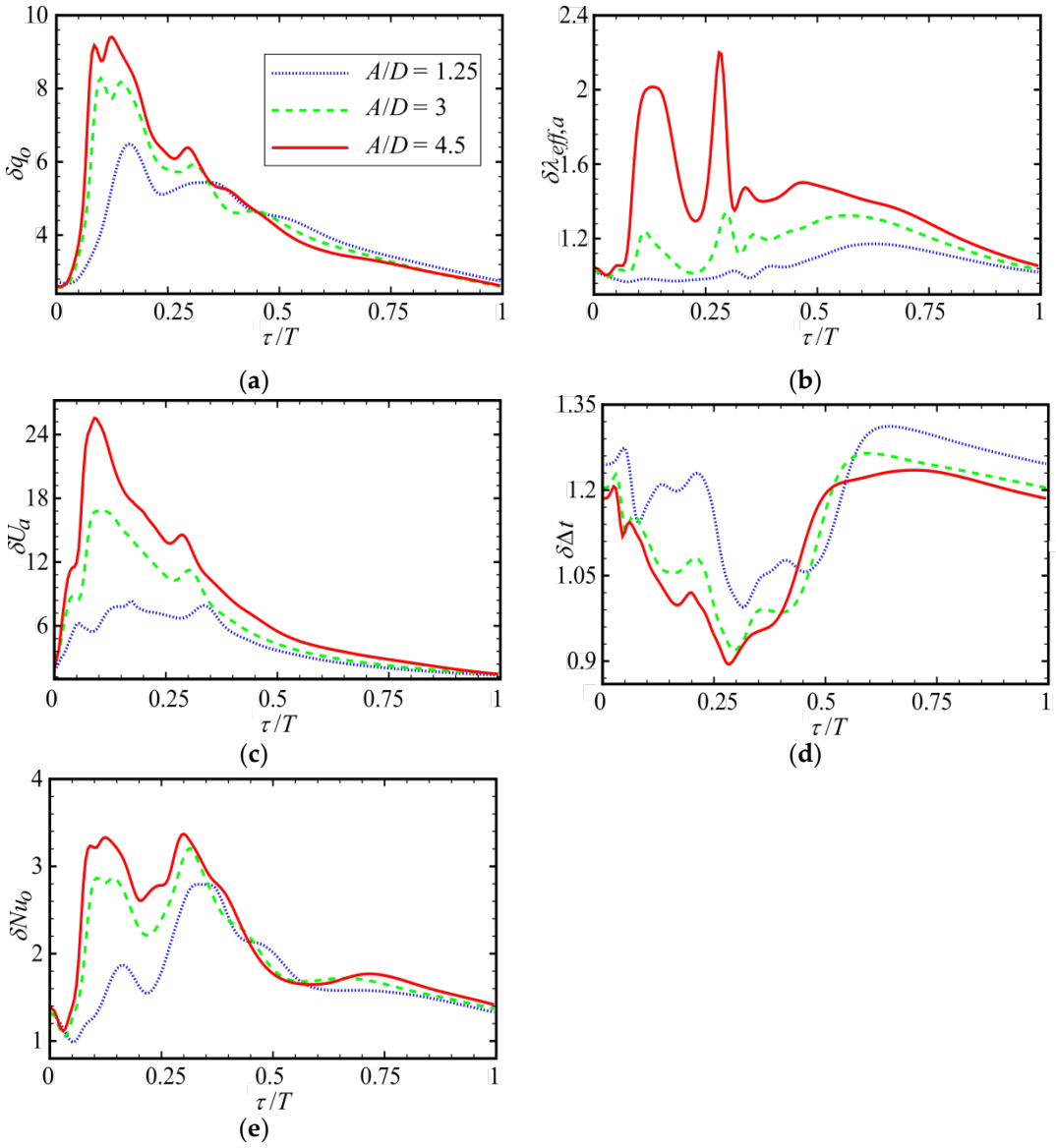

Figure 8. Effect of pulsations on instantaneous flow and heat transfer characteristics at $f = 0.5$ Hz for one period of pulsation: (**a**) Variation of δq_o with τ/T; (**b**) Variation of $\langle \delta\lambda_{eff,a} \rangle$ with τ/T; (**c**) Variation of $\langle \delta U_a \rangle$ with τ/T; (**d**) Variation of $\langle \delta\Delta t \rangle$ with τ/T; (**e**) Variation of $\langle \delta Nu_o \rangle$ with τ/T.

3.2. Effect of amplitude and frequency of pulsations on local flow characteristics and heat transfer

Figures 9-11 shows the variation of the local values of the heat flux $\langle \delta q_\varphi \rangle$, the effective thermal conductivity $\langle \delta\lambda_{eff,\varphi} \rangle$, the velocity $\langle \delta U_\varphi \rangle$ and the Nusselt number $\langle \delta Nu_\varphi \rangle$ with the amplitude A/D and the frequency f of pulsations. The maximum increase in velocity$\langle \delta U_\varphi \rangle$ in a pulsating flow with increase in the amplitude and frequency of pulsations (figure 9, (c), figure 10, (c)) is observed at $\varphi = 0°$ and 180°, which is consistent with increase in the local heat flux (figure 9, 10, (a)) and the Nusselt number (figure 11). In the A/D range from 3 to 4.5, a slight decline of the growth $\langle \delta U_\varphi \rangle$ is observed for $\varphi = 0°$ and 180° (figure 9, (c)), while the values of $\langle \delta q_\varphi \rangle$, $\langle \delta Nu_\varphi \rangle$ also declining at $\varphi = 180°$ and decreasing at $\varphi = 0°$ (figure 9, (a), (figure 11, (a)). The maximum growth of the effective thermal conductivity $\langle \delta\lambda_{eff,\varphi} \rangle$, with increasing A/D and f is observed at $\varphi = 45°$ (figure 9, 10 (b)), the minimum at $\varphi = 0°$ and 180°, which is opposite to $\langle \delta q_\varphi \rangle$, $\langle \delta Nu_\varphi \rangle$, $\langle \delta U_\varphi \rangle$. The maximum absolute values of $\langle \delta q_\varphi \rangle$, $\langle \delta Nu_\varphi \rangle$, $\langle \delta U_\varphi \rangle$ are observed at $\varphi = 0°$ and 180°, the minimum at $\varphi = 45°$ and 90°.

Preprints (www.preprints.org) | NOT PEER-REVIEWED | Posted: 30 June 2022 doi:10.20944/preprints202206.0419.v1

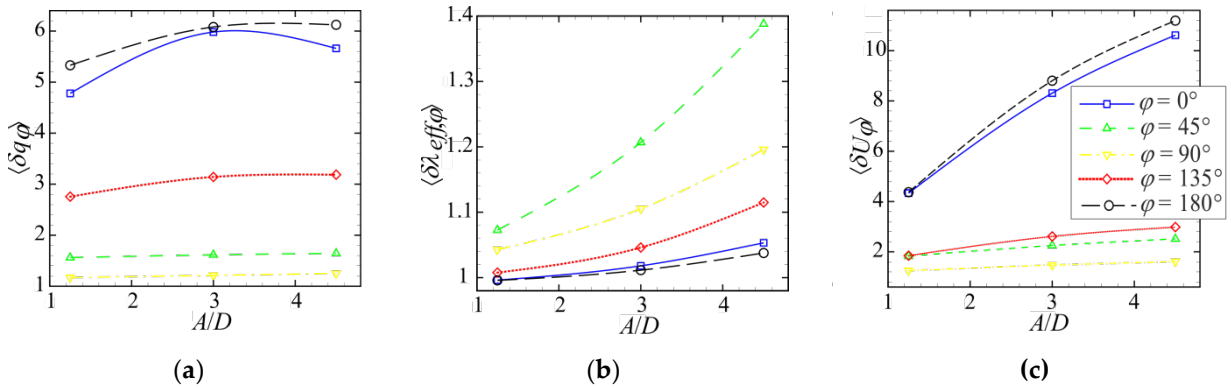

Figure 9. Effect of pulsations on local flow and heat transfer characteristics at $f = 0.25$ Hz: (**a**) Variation of $\langle \delta q_\varphi \rangle$ with A/D; (**b**) Variation of $\langle \delta \lambda_{eff,\varphi} \rangle$ with A/D; (**c**) Variation of $\langle \delta U_\varphi \rangle$ with A/D.

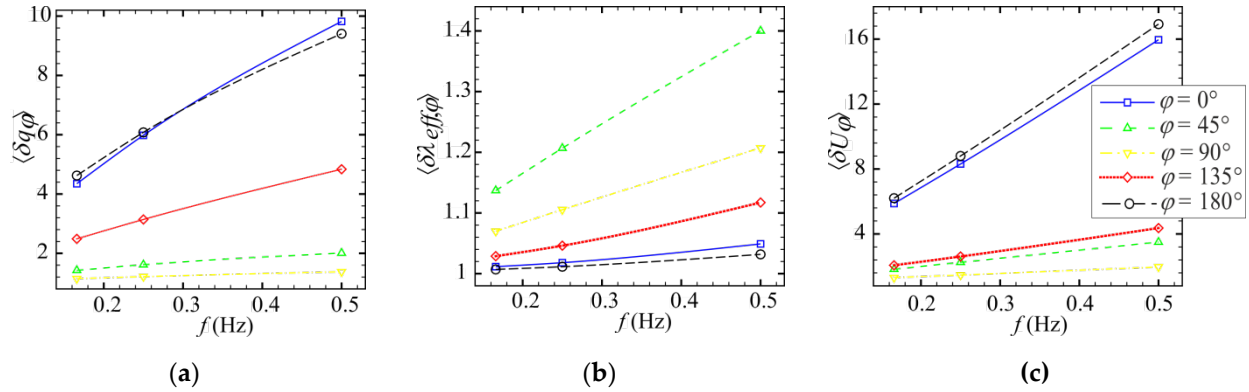

Figure 10. Effect of pulsations on local flow and heat transfer characteristics at $A/D = 3$: (**a**) Variation of $\langle \delta q_\varphi \rangle$ with f; (**b**) Variation of $\langle \delta \lambda_{eff,\varphi} \rangle$ with f; (**c**) Variation of $\langle \delta U_\varphi \rangle$ with f.

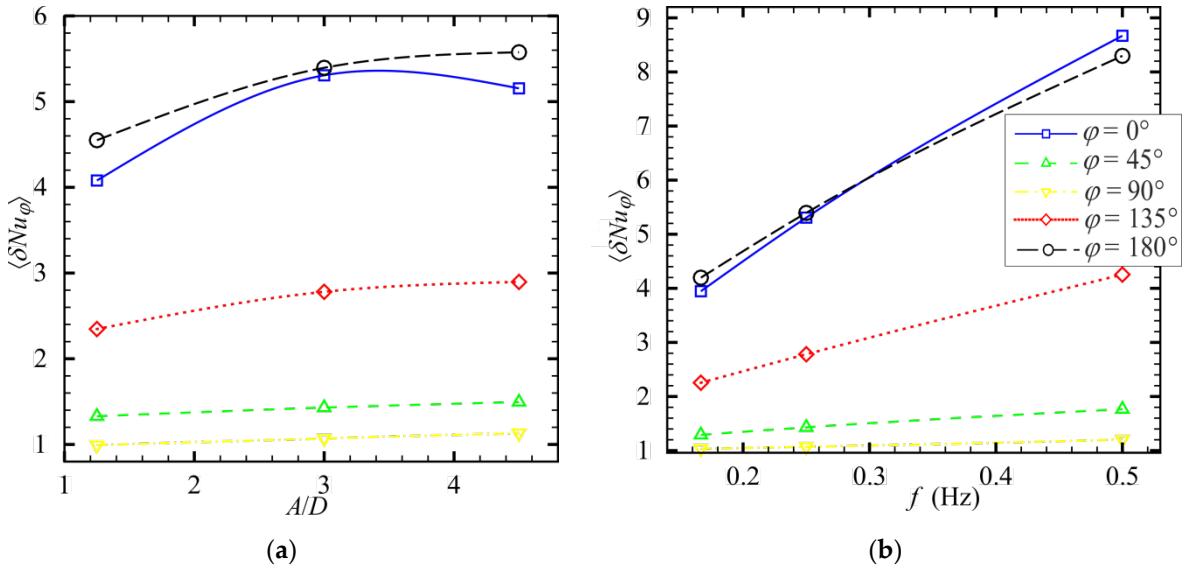

Figure 11. Effect of pulsations on local Nusselt number: (**a**) Variation of $\langle \delta Nu_\varphi \rangle$ with A/D at $f = 0.25$ Hz; (**b**) Variation of $\langle \delta Nu_\varphi \rangle$ with f at $A/D = 3$.

In the in-line tube bundles with a steady flow between the rows of the tube, regions with low circulation are formed. As a result, the heat transfer in these areas is reduced [32,33]. Increase in the intensity of pulsations leads to increase in the fluid circulation in these areas (Figure 9, 10, (c)). Therefore, with increase in the intensity of pulsations, increase in heat transfer occurs in the front ($\varphi = 0°$) and back ($\varphi = 180$) areas of the cylinder.

 doi:10.20944/preprints202206.0419.v1

The local dynamics of instantaneous values of δU_φ, δq_φ, δNu_φ, $\delta\lambda_{eff,\varphi}$ are shown in figure 12, 13. The values of local heat flux δq_φ and local Nusselt number δNu_φ in the front ($\varphi = 0°$) and back part ($\varphi = 135°$, 180°) of the cylinder are increasing up to 14-29 times, which is consistent with increase in the values of δU_φ.

For the instantaneous local effective thermal conductivity $\delta\lambda_{eff,\varphi}$ a rise to 1.4 is observed at $\varphi = 45°$, $A/D = 1.25$ (figure 13, (a)) during the second half-period T_2, while the instantaneous local Nusselt number δNu_φ at $\varphi = 45°$ does not increase (figure 13, (c)). Consequently, increase in $\delta\lambda_{eff,\varphi}$ to 1.4 is insufficient for heat transfer augmentation. It can be assumed that the heat transfer enhancement at $A/D = 1.25$ is mainly associated with increase in the flow velocity. When $A/D = 4.5$ instantaneous effective thermal conductivity $\delta\lambda_{eff,\varphi}$ increases up to 3.5 times, at $\varphi = 45°$, 90° and 135° figure 13, (b)), which is consistent with the growth of δq_φ and δNu_φ for this region of the cylinder.

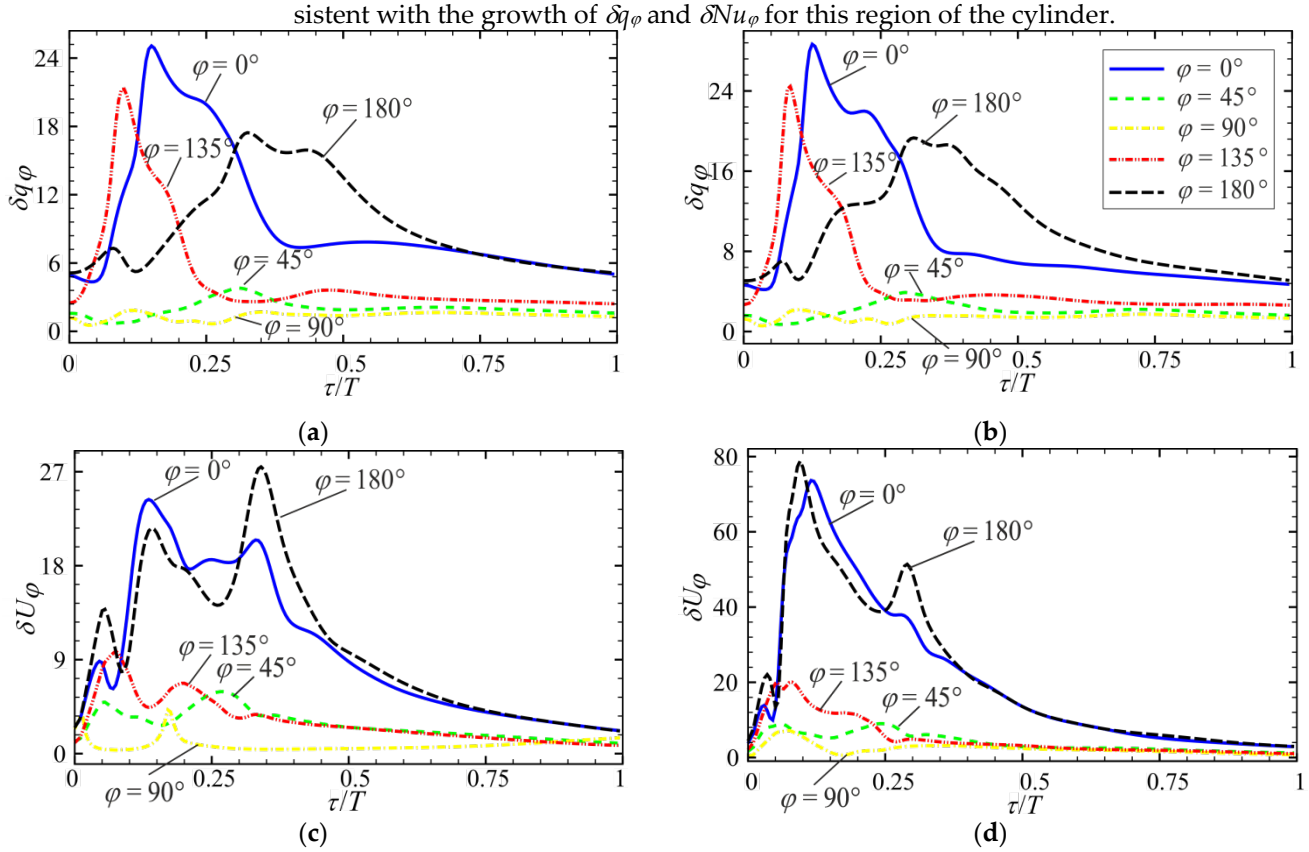

Figure 12. Effect of pulsations on instantaneous local heat flux and velocity at $f = 0.5$ Hz for on period of pulsation: (**a**) Variation of δq_φ with τ/T at $A/D = 1.25$; (**b**) Variation of δq_φ with τ/T at $A/D = 4.5$; (**c**) Variation of δU_φ with τ/T at $A/D = 1.25$; (**d**) Variation of δU_φ with τ/T at $A/D = 4.5$.

3.3. Contour plots of temperature, effective thermal conductivity, and plots of the velocity vector

Figures 14-16 show the instantaneous temperature contour plots, effective thermal conductivity, and velocity vectors for a steady flow. The plots are shown only for three central rows of the tube bundle. The temperature distribution and effective thermal conductivity are correlated with the velocity vectors. For example, the results show that two symmetric vortices are formed between the rows in the region φ = 135° and 225°. An increase in effective thermal conductivity is also observed in this region. At the front and back of the tubes, the flow velocity is close to zero, and the flow temperature is maximum, which is associated with poor flow circulation. Between the tubes (φ = 90°) the flow velocity is maximum and the temperature is minimum.

Preprints (www.preprints.org) | NOT PEER-REVIEWED | Posted: 30 June 2022 doi:10.20944/preprints202206.0419.v1

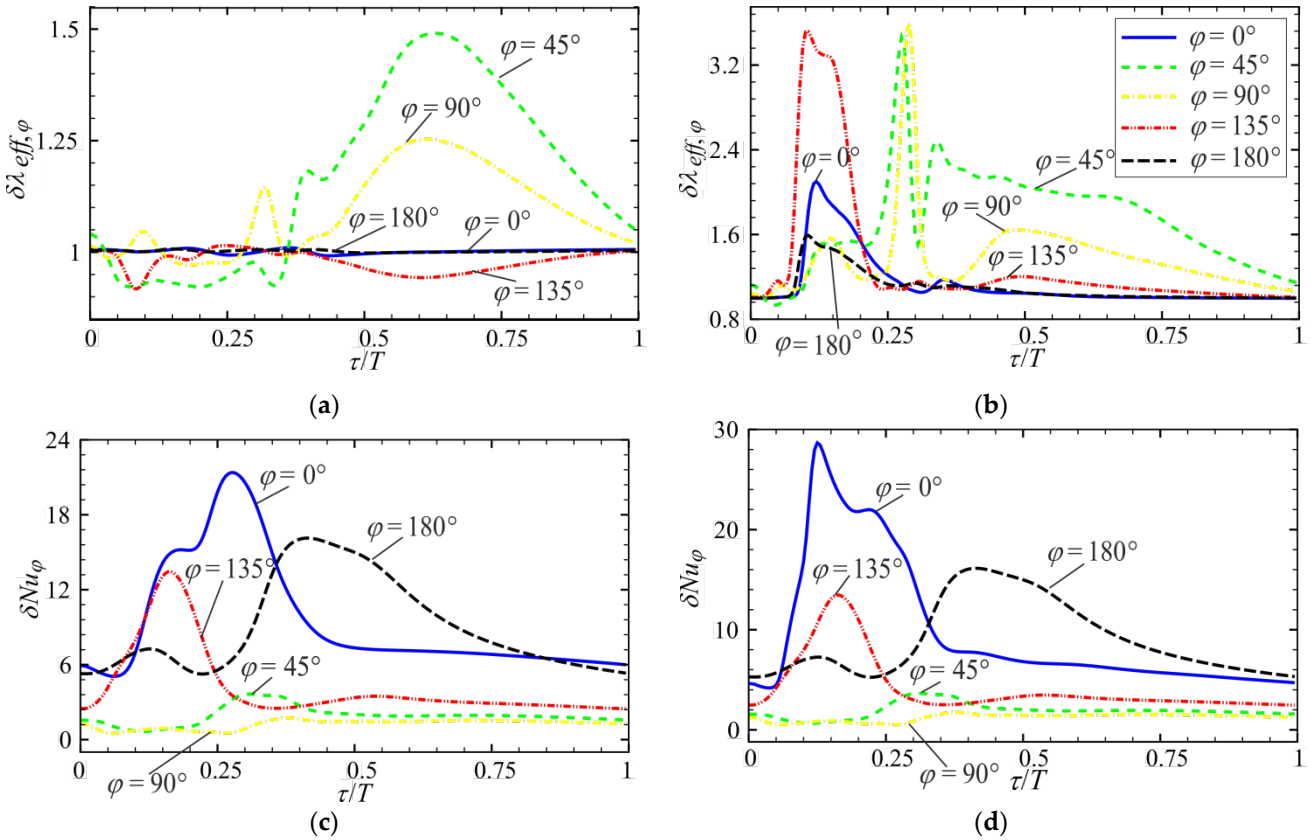

Figure 13. Effect of pulsations on instantaneous local heat flux and velocity at f = 0.5 Hz for on period of pulsation: (**a**) Variation of $\delta\lambda_{eff,\varphi}$ with τ/T at A/D = 1.25; (**b**) Variation of $\delta\lambda_{eff,\varphi}$ with τ/T at A/D = 4.5; (**c**) Variation of δNu_{φ} with τ/T at A/D = 1.25; (**d**) Variation of δNu_{φ} with τ/T at A/D = 4.5.

Figures 17-19 show the fields of temperatures, effective thermal conductivity, and velocity vectors at different phases of pulsations for three central rows of the tube bundle. Almost at all phases of pulsations, two symmetrical vortices are formed in the wake of tubes. The magnitude and size of the vortices increase with increasing input velocity. For phase (e), the size of the vortices between the rows is maximum; the formation of two additional smaller vortices in the region (φ = 0°, 180°) is also noticeable. The flow rate is maximum between tubes (φ = 90°) for phase (c). The increase in heat transfer is mainly associated with increased vortices size between the rows. The maximum heat transfer enhancement occurs in areas (φ = 0°, 180°) (figure 11). Molochnikov et al. [24] analyzed the flow structure and heat transfer in tube bundles at symmetric flow pulsations. Authors [24] reported maximum heat transfer enhancement during the formation of two symmetric vortices in the wake of the cylinder in the tube bundle, which is consistent with this work. Temperatures and effective thermal conductivity correlate with the flow distribution in a pulsating flow. For example, for phase (e), the maximum effective thermal conductivity is observed in the regions of vortex formation. The maximum effective thermal conductivity value is observed for phase (g).

Preprints (www.preprints.org) | NOT PEER-REVIEWED | Posted: 30 June 2022 doi:10.20944/preprints202206.0419.v1

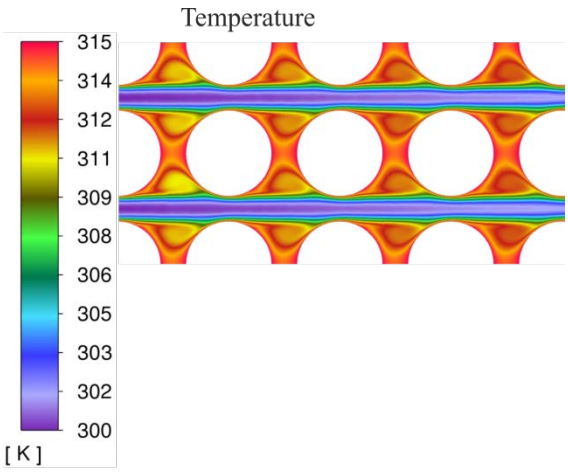

Figure 14. The temperature contour plots for three central rows of the tube bundle at a steady flow.

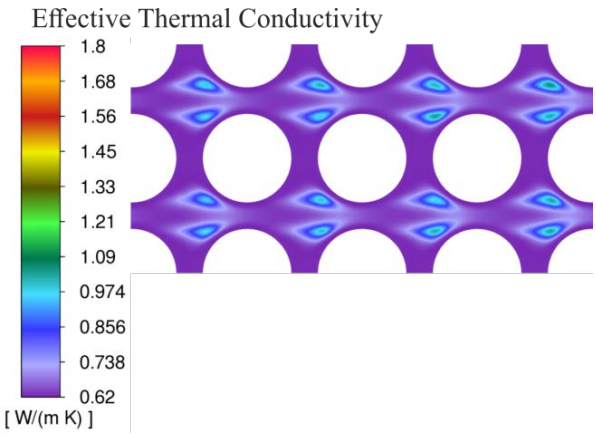

Figure 15. The effective thermal conductivity contour plots for three central rows of the tube bundle at a steady flow.

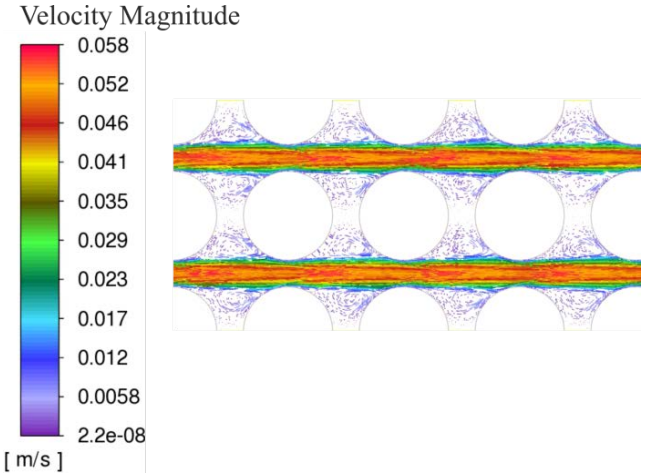

Figure 16. The velocity vectors plot for three central rows of the tube bundle at a steady flow.

Preprints (www.preprints.org) | NOT PEER-REVIEWED | Posted: 30 June 2022 doi:10.20944/preprints202206.0419.v1

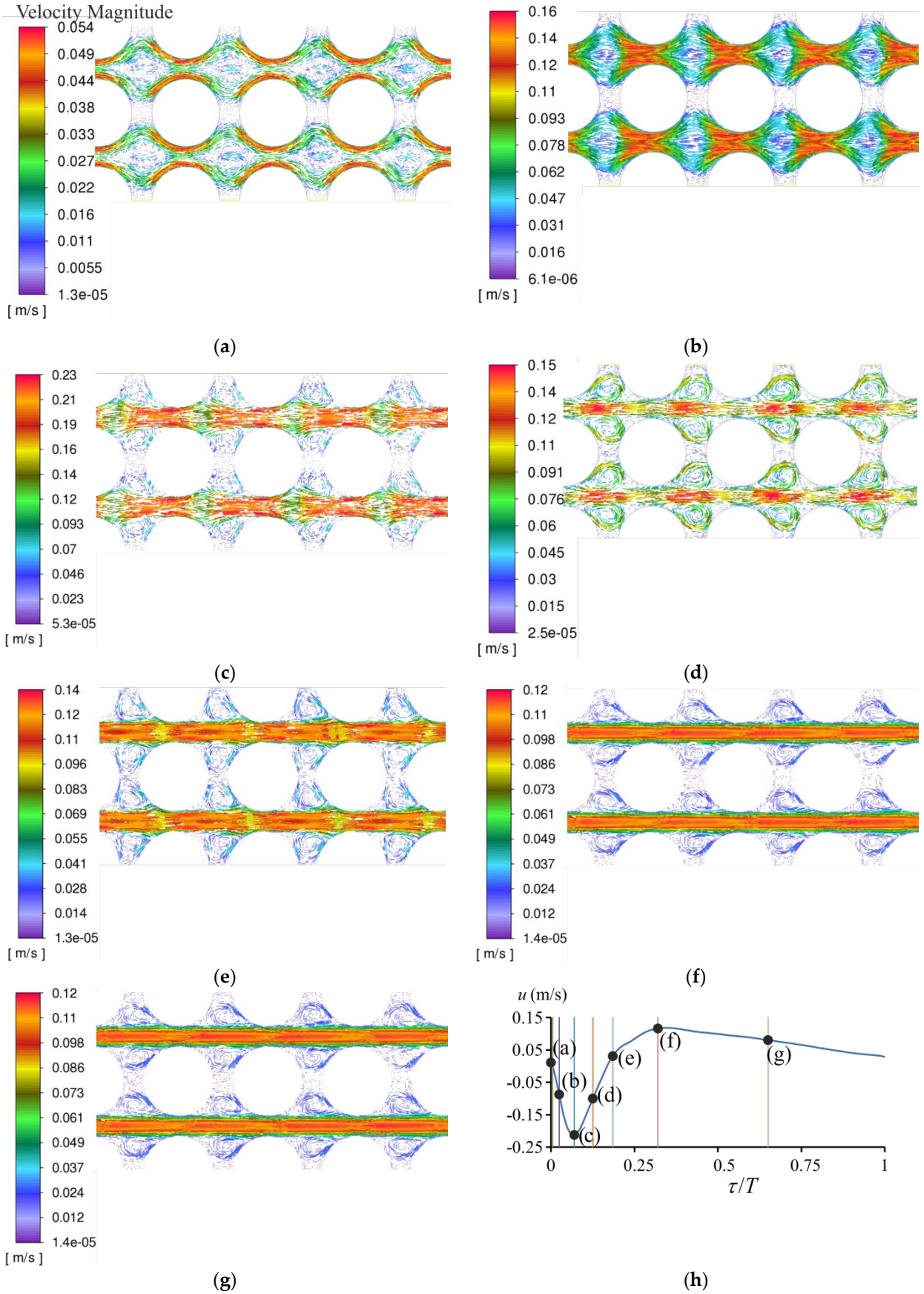

Figure 17. The instantaneous vectors plots at different phases of pulsations for three central rows of the tube bundle at $A/D = 3$, $f = 0.5$ Hz: (**a**) $\tau/T = 0.005$ (**b**) $\tau/T = 0.025$; (**c**) $\tau/T = 0.07$; (**d**) $\tau/T = 0.125$; (**e**) $\tau/T = 0.185$; (**f**) $\tau/T = 0.32$; (**g**) $\tau/T = 0.65$; (**h**) The velocity at tube bundle inlet for one period of pulsations and seven phase definition.

Preprints (www.preprints.org) | NOT PEER-REVIEWED | Posted: 30 June 2022 doi:10.20944/preprints202206.0419.v1

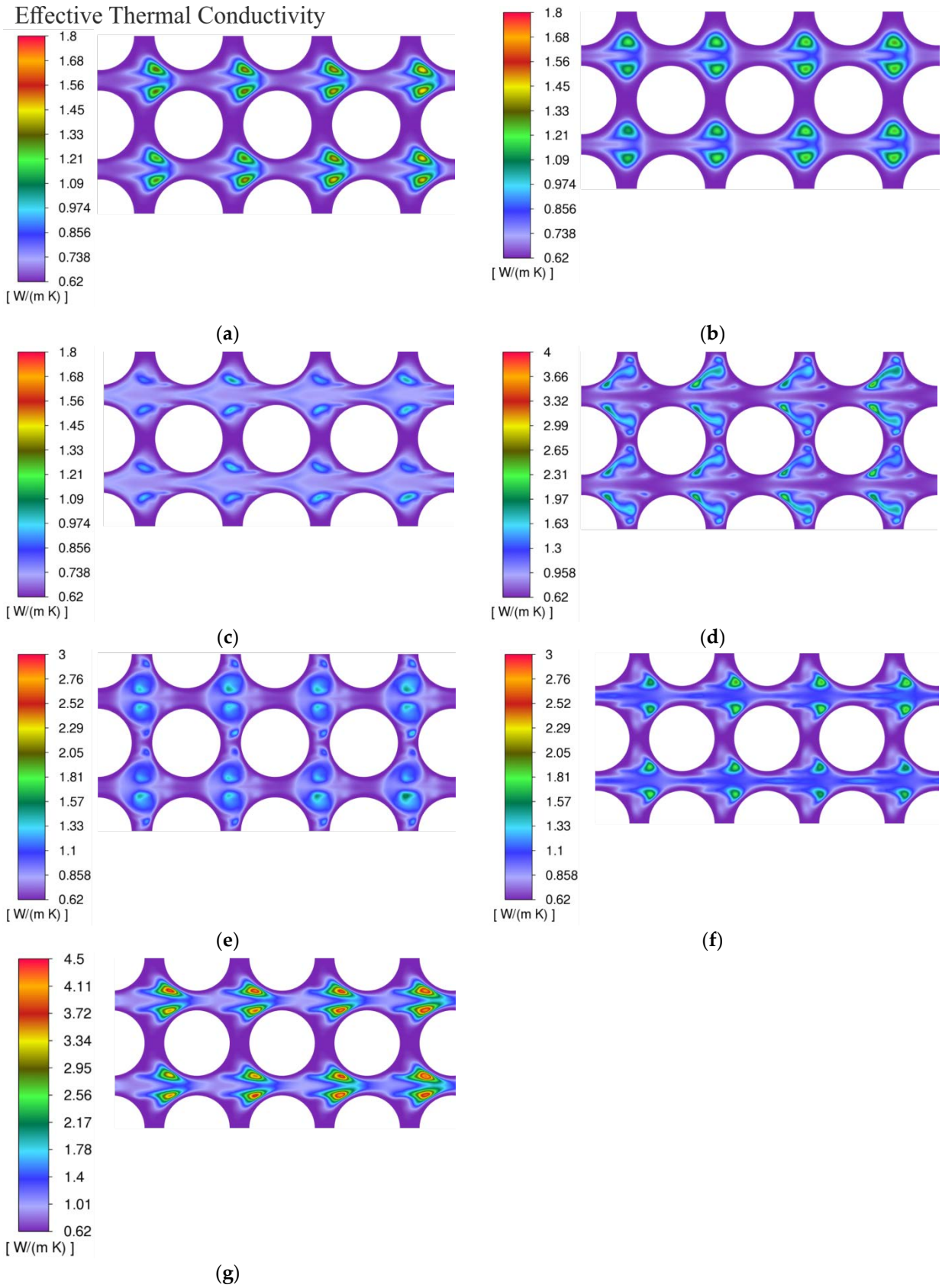

Figure 18. The instantaneous effective thermal conductivity contour plots at different phases of pulsations for three central rows of the tube bundle at $A/D = 3$, $f = 0.5$ Hz: (**a**) $\tau/T = 0.005$ (**b**) $\tau/T = 0.025$; (**c**) $\tau/T = 0.07$; (**d**) $\tau/T = 0.125$; (**e**) $\tau/T = 0.185$; (**f**) $\tau/T = 0.32$; (**g**) $\tau/T = 0.65$.

Preprints (www.preprints.org) | NOT PEER-REVIEWED | Posted: 30 June 2022 doi:10.20944/preprints202206.0419.v1

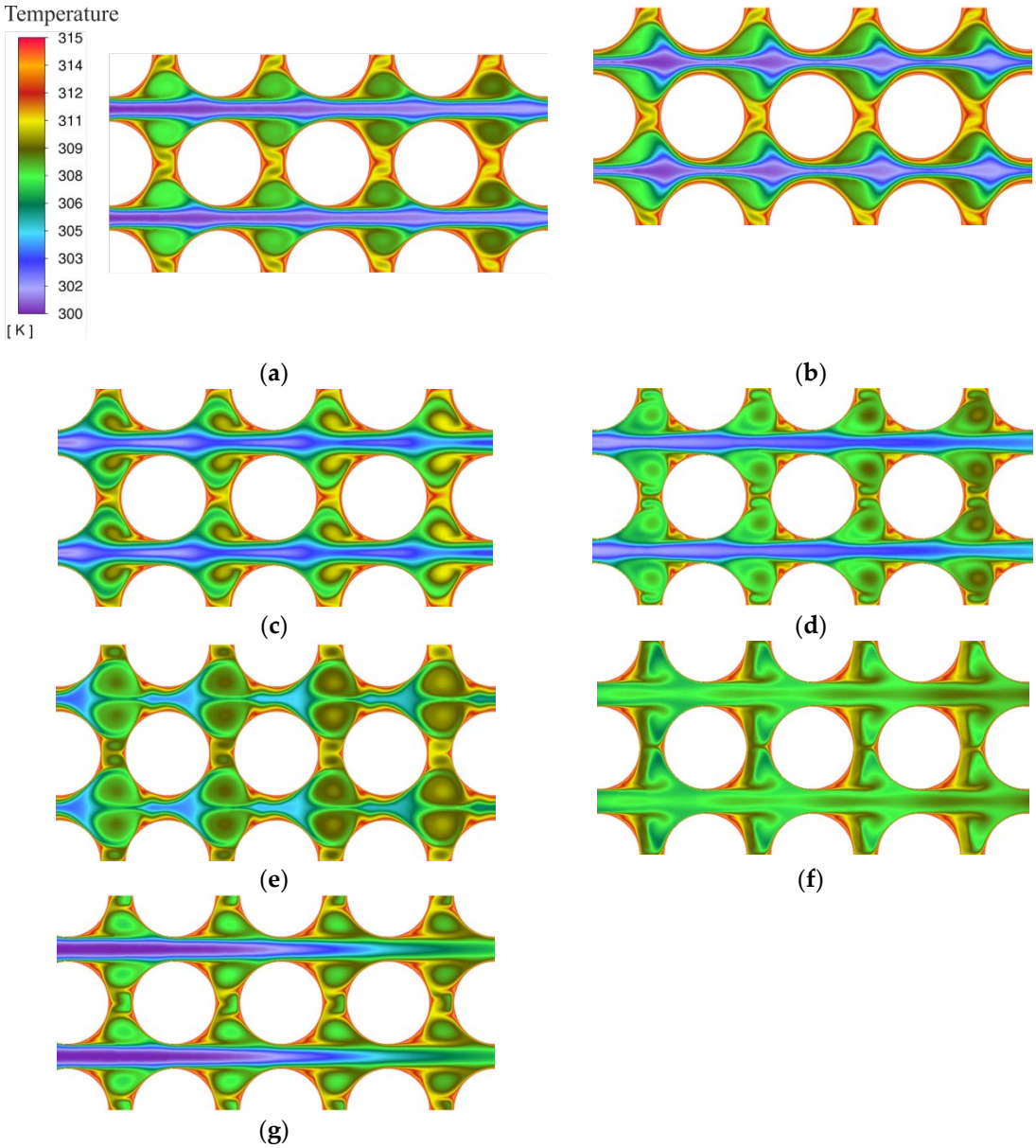

Figure 19. The instantaneous temperature contour plots at different phases of pulsations for three central rows of the tube bundle at A/D = 3, f = 0.5 Hz: (**a**) τ/T = 0.005 (**b**) τ/T = 0.025; (**c**) τ/T = 0.07; (**d**) τ/T = 0.125; (**e**) τ/T = 0.185; (**f**) τ/T = 0.32; (**g**) τ/T = 0.65.

5. Conclusions

In this work, the effect of asymmetric pulsating flows on the dynamics of the heat transfer and flow characteristics around the central cylinder in an in-line tube bundle is considered. Increase in the frequency and the amplitude of pulsations leads to a heat transfer enhancement. The heat transfer enhancement in a pulsating flow is mainly associated with increase in the local flow velocity. With increase in the frequency and amplitude of pulsations, increase in the flow velocity occurs. The increased flow velocity leads to increase in the size of vortices between the rows of the tube bundle and the formation of two additional smaller vortices. Increase in the size and velocity of vortices between the rows of the tube bundle is responsible for heat transfer enhancement. The maximum velocity augmentation is observed in the front ($\varphi = 0°$) and back of the cylinder ($\varphi = 180°$), consistent with heat transfer augmentation in these areas. The maximum effective thermal conductivity augmentation is observed at $\varphi = 45°$. The effective thermal conductivity increases with increase in the pulsation amplitude. Still, it practically does

not change with increased pulsation frequency, although the heat transfer augmentation is always associated with higher frequency. Therefore, it follows that the effective thermal conductivity does not significantly affect heat transfer enhancement. The maximum increase in heat transfer during pulsations occurs when the flow velocity has maximum acceleration.

Further studies will be aimed at studying the mechanisms of heat transfer enhancement during pulsating flows in tube bundles with tube bundle configurations different from this work and Reynolds numbers Re > 1000.

Author Contributions: Conceptualization, A.H. and A.K.; methodology, V.B., L.K., D.B. and V.I.; software, A.K.; validation, V.B. and L.K.; investigation, A.H., V.B. and L.K.; formal analysis, V.B., L.K., D.B. and V.I., writing—original draft preparation, A.H. and A.K.; writing—review and editing, A.H., D.B. and V.I.; visualization, A.K. and D.B.; supervision, A.H.; project administration, A.H. All authors have read and agreed to the published version of the manuscript.

Funding: This research was funded by the Russian Science Foundation, grant number 18-79-10136.

Conflicts of Interest: The authors declare no conflict of interest.

References

1. Bergles, A.E.; Manglik, R.M. CURRENT PROGRESS AND NEW DEVELOPMENTS IN ENHANCED HEAT AND MASS TRANSFER. *Journal of Enhanced Heat Transfer* **2013**, *20*, 1-15.
2. Alam, T.; Kim, M.-H. A comprehensive review on single phase heat transfer enhancement techniques in heat exchanger applications. Renewable and Sustainable Energy Reviews 2018, 81, 813-839, doi:10.1016/j.rser.2017.08.060.
3. Wang, W.; Shuai, Y.; Li, B.; Li, B.; Lee, K.-S. Enhanced heat transfer performance for multi-tube heat exchangers with various tube arrangements. International Journal of Heat and Mass Transfer 2021, 168, 120905, doi:10.1016/j.ijheatmasstransfer.2021.120905.
4. Nguyen, D.H.; Ahn, H.S. A comprehensive review on micro/nanoscale surface modification techniques for heat transfer enhancement in heat exchanger. International Journal of Heat and Mass Transfer 2021, 178, 121601, doi:10.1016/j.ijheatmasstransfer.2021.121601.
5. Maradiya, C.; Vadher, J.; Agarwal, R. The heat transfer enhancement techniques and their Thermal Performance Factor. Beni-Suef University Journal of Basic and Applied Sciences 2018, 7, 1-21, doi:10.1016/j.bjbas.2017.10.001.
6. Li, X.; Zhu, D.; Sun, J.; Mo, X.; Liu, S. Heat transfer and pressure drop for twisted oval tube bundles with staggered layout in crossflow of air. Applied Thermal Engineering 2019, 148, 1092-1098, doi:10.1016/j.applthermaleng.2018.11.124.
7. Khalatov, A.A.; Kovalenko, G.V.; Meiris, A.Z. Heat Transfer in Air Flow Across a Single-Row Bundle of Tubes With Spiral Grooves. Journal of Engineering Physics and Thermophysics 2018, 91, 64-71, doi:10.1007/s10891-018-1719-x.
8. Pongsoi, P.; Pikulkajorn, S.; Wongwises, S. Effect of fin pitches on the optimum heat transfer performance of crimped spiral fin-and-tube heat exchangers. International Journal of Heat and Mass Transfer 2012, 55, 6555-6566, doi:10.1016/j.ijheatmasstransfer.2012.06.061.
9. Mavridou, S.G.; Konstandinidis, E.; Bouris, D.G. Experimental evaluation of pairs of inline tubes of different size as components for heat exchanger tube bundles. International Journal of Heat and Mass Transfer 2015, 90, 280-290, doi:10.1016/j.ijheatmasstransfer.2015.06.047.
10. Wangnipparnto, S.; Tiansuwan, J.; Kiatsiriroat, T.; Wang, C.C. Performance analysis of thermosyphon heat exchanger under electric field. Energy Conversion and Management 2003, 44, 1163-1175, doi:10.1016/s0196-8904(02)00104-8.
11. Cheng, L.; Luan, T.; Du, W.; Xu, M. Heat transfer enhancement by flow-induced vibration in heat exchangers. International Journal of Heat and Mass Transfer 2009, 52, 1053-1057, doi:10.1016/j.ijheatmasstransfer.2008.05.037.
12. Jeng, T.-M.; Tzeng, S.-C.; Xu, R. Heat transfer characteristics of a rotating cylinder with a lateral air impinging jet. International Journal of Heat and Mass Transfer 2014, 70, 235-249, doi:10.1016/j.ijheatmasstransfer.2013.10.069.

13. Cheng, P.; Zhao, T.S. HEAT TRANSFER IN OSCILLATORY FLOWS. Annual Review of Heat Transfer 1998, 9, 359-420, doi:10.1615/annualrevheattransfer.v9.90.
14. Herman, C. THE IMPACT OF FLOW OSCILLATIONS ON CONVECTIVE HEAT TRANSFER. Annual Review of Heat Transfer 2000, 11, 495-561, doi:10.1615/annualrevheattransfer.v11.100.
15. Elshafei, E.A.M.; Safwat Mohamed, M.; Mansour, H.; Sakr, M. Experimental study of heat transfer in pulsating turbulent flow in a pipe. International Journal of Heat and Fluid Flow 2008, 29, 1029-1038, doi:10.1016/j.ijheatfluidflow.2008.03.018.
16. Olayiwola, B.; Walzel, P. Cross-flow transport and heat transfer enhancement in laminar pulsed flow. Chemical Engineering and Processing: Process Intensification 2008, 47, 929-937, doi:10.1016/j.cep.2007.02.009.
17. Kikuchi, Y.; Suzuki, H.; Kitagawa, M.; Ikeya, K.-I. Effect of Pulsating Strouhal Number on Heat Transfer around a Heated Cylinder in Pulsating Cross-Flow. JSME International Journal Series B 2000, 43, 250-257, doi:10.1299/jsmeb.43.250.
18. Fu, W.-S.; Tong, B.-H. Numerical investigation of heat transfer from a heated oscillating cylinder in a cross flow. International Journal of Heat and Mass Transfer 2002, 45, 3033-3043, doi:10.1016/s0017-9310(02)00016-9.
19. Zheng, Y.; Li, G.; Guo, W.; Dong, C. Lattice Boltzmann simulation to laminar pulsating flow past a circular cylinder with constant temperature. Heat and Mass Transfer 2017, 53, 2975-2986, doi:10.1007/s00231-017-2043-2.
20. Ji, T.H.; Kim, S.Y.; Hyun, J.M. Experiments on heat transfer enhancement from a heated square cylinder in a pulsating channel flow. International Journal of Heat and Mass Transfer 2008, 51, 1130-1138, doi:10.1016/j.ijheatmasstransfer.2007.04.015.
21. Luo, X.; Zhang, W.; Dong, H.; Thakur, A.K.; Yang, B.; Zhao, W. Numerical analysis of heat transfer enhancement of fluid past an oscillating circular cylinder in laminar flow regime. Progress in Nuclear Energy 2021, 139, 103853, doi:10.1016/j.pnucene.2021.103853.
22. Mikheev, N.I.; Molochnikov, V.M.; Mikheev, A.N.; Dushina, O.A. Hydrodynamics and heat transfer of pulsating flow around a cylinder. International Journal of Heat and Mass Transfer 2017, 109, 254-265, doi:10.1016/j.ijheatmasstransfer.2017.01.125.
23. Molochnikov, V.M.; Mikheev, N.I.; Mikheev, A.N.; Paereliy, A.A. Heat transfer from a cylinder in pulsating cross-flow. Thermophysics and Aeromechanics 2017, 24, 569-575, doi:10.1134/s0869864317040084.
24. Molochnikov, V.M.; Mikheev, A.N.; Aslaev, A.K.; Dushina, O.A.; Paereliy, A.A. Heat transfer of a tube bundle in a pulsating flow. Thermophysics and Aeromechanics 2019, 26, 547-559, doi:10.1134/s0869864319040073.
25. Molochnikov, V.M.; Mikheev, A.N.; Aslaev, A.K.; Goltsman, A.E.; Paereliy, A.A.; Iop. Flow structure between the tubes and heat transfer of a tube bundle in pulsating flow. In Proceedings of the All-Russian Conference / 34th Siberian Thermophysical Seminar (STS) dedicated to the 85th anniversary of Academician A. K. Rebrov, Russian Acad Sci, Siberian Branch, Kutateladze Inst Thermophys, Novosibirsk, RUSSIA, Aug 27-30, 2018.
26. Liang, C.L.; Papadakis, G. Study of the effect of flow pulsation on the flow field and heat transfer over an inline cylinder array using LES. Engineering Turbulence Modelling and Experiments 6 2005, 813-822, doi:10.1016/b978-008044544-1/50078-9.
27. Wu, Z.; You, S.; Zhang, H.; Zheng, W. Experimental investigation on heat transfer characteristics of staggered tube bundle heat exchanger immersed in oscillating flow. International Journal of Heat and Mass Transfer 2020, 148, 119125, doi:10.1016/j.ijheatmasstransfer.2019.119125.
28. Chen, S.; Huang, Q.; Liang, M.; Chen, H.; Chen, L.; Hou, Y. Numerical study on the heat transfer characteristics of oscillating flow in cryogenic regenerators. Cryogenics 2018, 96, 99-107, doi:10.1016/j.cryogenics.2018.10.012.
29. Mulcahey, T.I.; Pathak, M.G.; Ghiaasiaan, S.M. The effect of flow pulsation on drag and heat transfer in an array of heated square cylinders. International Journal of Thermal Sciences 2013, 64, 105-120, doi:10.1016/j.ijthermalsci.2012.08.017.
30. Balabani, S.; Yianneskis, M. An experimental study of the mean flow and turbulence structure of cross-flow over tube bundles. Proceedings of the Institution of Mechanical Engineers Part C-Journal of Mechanical Engineering Science 1996, 210, 317-331, doi:10.1243/pime_proc_1996_210_204_02.
31. Shah, R.K.; Sekulić, D.P. Fundamentals of Heat Exchanger Design; 2003.

32. Zhukauskas, A.A.; Ulinskas, R. Heat transfer of banks of tubes in crossflow; Mokslas: 1986; p. 200. (In Russian)
33. Zukauskas, A. Heat Transfer from Tubes in Crossflow. Advances in heat transfer 1972, 18, 87-159.
34. Ye, Q.; Zhang, Y.; Wei, J. A comprehensive review of pulsating flow on heat transfer enhancement. Applied Thermal Engineering 2021, 196, 117275, doi:10.1016/j.applthermaleng.2021.117275.
35. Sung, H.J.; Hwang, K.S.; Hyun, J.M. EXPERIMENTAL-STUDY ON MASS-TRANSFER FROM A CIRCULAR-CYLINDER IN PULSATING FLOW. International Journal of Heat and Mass Transfer 1994, 37, 2203-2210, doi:10.1016/0017-9310(94)90363-8.
36. Cheng, C.-H.; Hong, J.-L.; Aung, W. Numerical prediction of lock-on effect on convective heat transfer from a transversely oscillating circular cylinder. International Journal of Heat and Mass Transfer 1997, 40, 1825-1834, doi:10.1016/s0017-9310(96)00255-4.
37. Konstantinidis, E.; Balabani, S.; Yianneskis, M. Relationship Between Vortex Shedding Lock-On and Heat Transfer. Chemical Engineering Research and Design 2003, 81, 695-699, doi:10.1205/026387603322150543.
38. Perwaiz, J.; Base, T.E. HEAT-TRANSFER FROM A CYLINDER AND FINNED TUBE IN A PULSATING CROSS-FLOW. Experimental Thermal and Fluid Science 1992, 5, 506-512, doi:10.1016/0894-1777(92)90037-6.
39. Ilyin, V.K.; Sabitov, L.S.; Haibullina, A.I.; Hayrullin, A.R.; IOP. Factors influencing on the thermal flow with the cross-section of the corridor tube bundle in low-frequency non-symmetric pulsations. In International Scientific-Technical Conference on Innovative Engineering Technologies, Equipment and Materials 2016 (Istc-Ietem-2016); 2017; Volume 240.
40. Abramov, A.G.; Levchenya, A.M.; Smirnov, E.M.; Smirnov, P.E. Numerical simulation of liquid metal turbulent heat transfer from an inline tube bundle in cross-flow. St. Petersburg Polytechnical University Journal: Physics and Mathematics 2015, 1, 356-363, doi:10.1016/j.spjpm.2016.02.002.
41. Ivanov, N.G.; Kirillov, A.I.; Smirnov, E.M.; Ris, V.V. Numerical Modeling of Buoyancy-Induced Fluid Flow and Heat Transfer in a Staggered Tube Bank. In Proceedings of the 2010 14th International Heat Transfer Conference, 2010; pp. 545-551.
42. Hajbullina, A.; Hajrullin, A.; Il'in, V. Heat transfer in the flow channel in tube bundle corridor type under imposed on the flow liquid of upstream low-frequency asymmetrical pulsations. Power engineering: research, equipment, technology 2016, 56-67, (In Russian) doi:10.30724/1998-9903-2016-0-11-12-56-67.
43. Larock, B.E.; Jeppson, R.W.; Watters, G.Z. Hydraulics of Pipeline Systems; CRC Press: 2000.
44. Spalart, P.; Allmaras, S. A One-Equation Turbulence Model for Aerodynamic Flow. AIAA 1992, 439.
45. Wang, Y.Q.; Jackson, P.L. Turbulence Modeling Applied to Flow Through a Staggered Tube Bundle. Journal of Thermophysics and Heat Transfer 2010, 24, 534-543, doi:10.2514/1.44356.
46. Kim, S.-M.; Ghiaasiaan, S.M. Numerical Modeling of Laminar Pulsating Flow in Porous Media. Journal of Fluids Engineering 2009, 131, 041203, doi:10.1115/1.3089541.
47. Haibullina, A.I. Improving the efficiency of heat exchangers due to low-frequency flow pulsations. Cand. Sc. (Technology) Thesis, Kazan State Power Engineering University, Kazan, 2017. (In Russian)